

METHODOLOGICAL NOTES

PACS numbers: **71.27. + a, 73.22. – f, 75.47. – m**

On the problem of detecting Majorana fermions in heat capacity and Hall effect measurements in the Kondo insulator YbB_{12}

A N Azarevich, A V Bogach, S Yu Gavrilkin, S V Demishev, N E Sluchanko

DOI: https://doi.org/10.3367/UFNe.2023.06.039405

Contents

Abstract. **We show that the separation of contributions to low-temperature heat capacity and the Hall effect, carried out in *Phys. Rev. Lett.* 120 257206 (2018), *Nat. Phys.* 15 954 (2019), *Phys. Rev. X* 12 021050 (2022), leads to unfounded conclusions about (i) the formation of uncharged quasiparticles (Majorana fermions) and (ii) the transition, as the magnetic field increases, to the metallic state with heavy fermions in the YbB_{12} semiconductor with strong electronic correlations. We obtain an alternative explanation of the experimental data in terms of the filamentary structure of conducting channels in the semiconductor matrix of ytterbium-based dodecaborides. Such channels (charge stripes) are nanoscale electron-density inhomogeneities and form manybody states near the Fermi level.**

Keywords: Kondo insulators, electronic phase separation, dynamical charge stripes

A N Azarevich [(1, 2, a)], **A V Bogach** [(1, b)], **S Yu Gavrilkin** [(3, c)], **S V Demishev** [(1, 4, 5, d)], **N E Sluchanko** [(1, e)]
[(1)] Prokhorov General Physics Institute, Russian Academy of Sciences, ul. Vavilova 38, 119991 Moscow, Russian Federation
[(2)] Moscow Institute of Physics and Technology (National Research University), Institutskii per. 9, 141701 Dolgoprudny, Moscow region, Russian Federation
[(3)] Lebedev Physical Institute, Russian Academy of Sciences, Leninskii prosp. 53, 119991 Moscow, Russian Federation
[(4)] Vereshchagin Institute for High Pressure Physics, Russian Academy of Sciences, Kaluzhskoe shosse 14, 108840 Troitsk, Moscow, Russian Federation
[(5)] HSE University, ul. Myasnitskaya 20, 101000 Moscow, Russian Federation
E-mail: [(a)] azarevich@lt.gpi.ru, [(b)] alex@lt.gpi.ru, [(c)] gavrilkinsy@lebedev.ru, [(d)] demishev@hppi.troitsk.ru, [(e)] nes@lt.gpi.ru

Received 25 May 2023
Uspekhi Fizicheskikh Nauk **194** (3) 336 – 343 (2024)
Translated by S Alekseev

1. Introduction

It is commonly believed that the YbB_{12} compound is a classic example of a system with strong electron correlations and is a topological Kondo insulator [1–3]. In this narrow-gap semiconductor with a mixed valence of ytterbium $v(\mathrm{Yb}) = 2.9$–2.95 [4–8], manybody states are detected in the $\Delta E_g/k_B \approx 18$ meV gap [9–10] in the vicinity of the Fermi level E_F in the energy range of 1–6 meV; the nature of these states is still the subject of active debate (see, e.g., [10–15]). The exotic electronic properties recently discovered at low and ultra-low temperatures in the dielectric state of YbB_{12} include quantum oscillations of magnetization and resistivity, usually characteristic of a normal metal with a three-dimensional Fermi surface, and very unusual *gapless charge-neutral fermion excitations* [11–15]. To explain the nature of these *uncharged fermions* in YbB_{12}, several models have been proposed based on a system of Majorana fermions with a gapless three-dimensional dielectric state [16–19]. The description of YbB_{12} proposed in recent theoretical studies invokes topologically protected gapless Majorana fermions arising due to phase shifts of bands in a mixed-valence insulator [20]. In [21], in addition, the ground state of the Landau Fermi liquid, containing Majorana polarons in the Kondo insulator phase, was studied. We also note recent studies [22–24], which suggest the separation of spins and charges in mixed-valence compounds: the appearance of uncharged fermions interacting with the U(1) gauge field then causes their hybridization, giving rise to the formation of composite excitons [23].

2. Heat capacity of YbB_{12} in a zero field

We emphasize that, for the models listed above of fundamental importance, is the conclusion about a finite (nonzero) density of states at the Fermi level $N(E_F)$ in the dielectric state of YbB_{12}, a conclusion arrived at in [11, 15] based on results of analyses of heat capacity at low temperatures $T \leqslant 14$ K (Fig. 1). In particular, in [11, 15], in analyzing the heat capacity in the range of 1–14 K, it was proposed that its phonon part C_{ph}, be decomposed into two Einstein contribu-

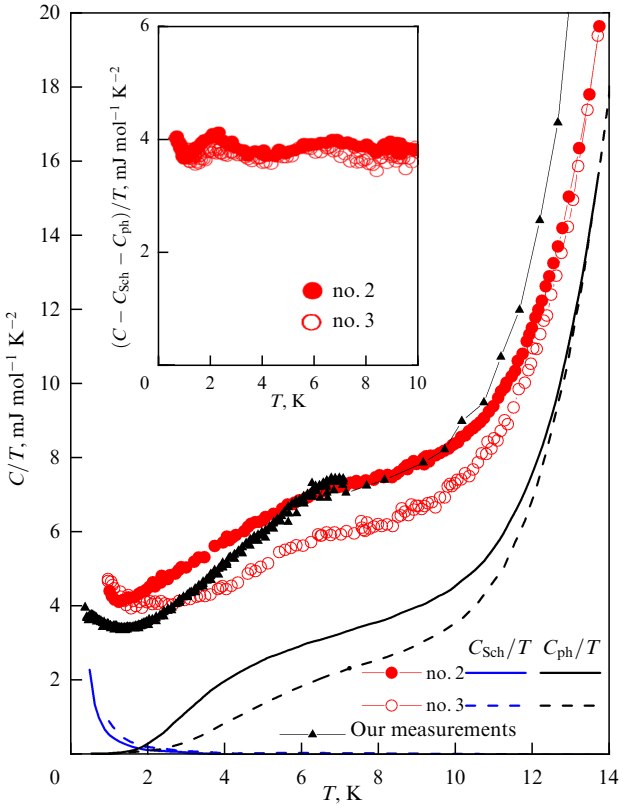

Figure 1. Temperature dependence of YbB_{12} heat capacity normalized by temperature in a zero field for single crystals no. 2 and no. 3, constructed from data in [11, 15], compared with results of our measurements. Black solid and dashed lines for crystals no. 2 and no. 3, respectively, show phonon heat capacity C_{ph}, represented by authors of [11, 15] as the sum of two Einstein components $C_{E1} + C_{E2}$ and a Debye component $C_D = \beta T^3$; blue solid and dashed lines show low-temperature Schottky contributions C_{Sch}. Inset shows quasiparticle contribution C_{qp}/T obtained in [11, 15] for crystals no. 2 and no. 3 by subtracting phonon and Schottky contributions from the total heat capacity.

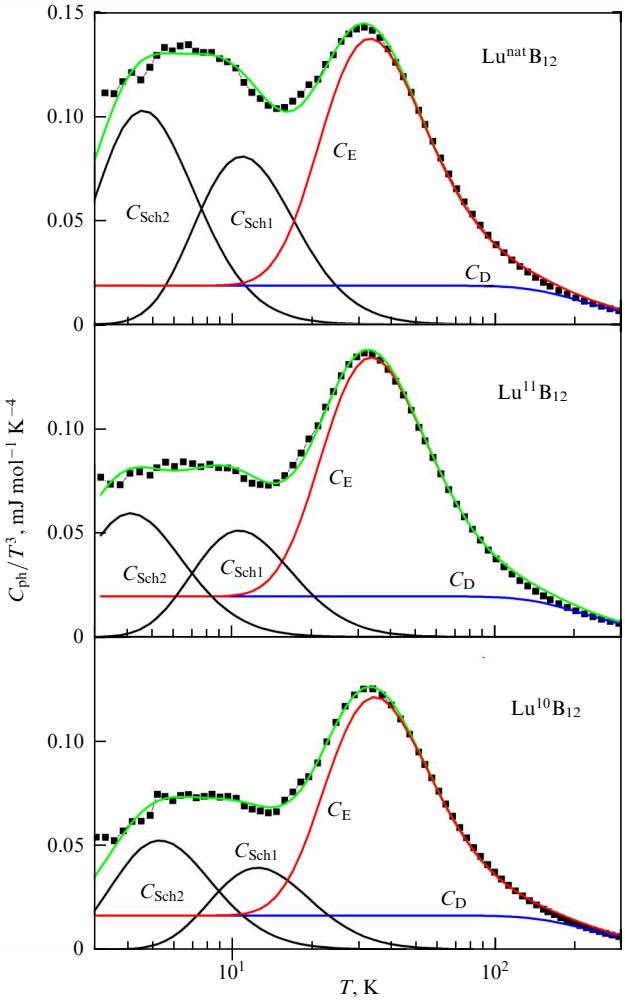

Figure 2. Temperature dependences of heat capacity $C_{ph} = C - \gamma T$ in coordinates $C_{ph}/T^3 = f(T)$ in a zero field for LuB_{12} single crystals with different boron isotopic compositions (constructed in accordance with data in [26]). Einstein (C_E), Debye (C_D), and two Schottky (C_{Sch1} and C_{Sch2}) contributions are shown with respective red, blue, and black solid lines. Approximation C_{ph}/T^3 (green curves) corresponds to Sommerfeld coefficient $\gamma = 3$ mJ mol^{-1} K^{-2}; Debye temperature values in range $\Theta_D = 1060$–1130 K (C_D contribution) depending on the boron isotopic composition were obtained in [26] directly from X-ray diffraction analysis of root-mean-square displacements of boron atoms.

tions $C_{E1} + C_{E2}$ and a Debye contribution $C_D = \beta T^3$, with the very small Schottky contribution C_{Sch} and the linear 'Sommerfeld' term $C_{qp} = \gamma T$ taken into account. The latter describes the component corresponding to quasiparticles in YbB_{12}, which are *gapless uncharged* (*Majorana*) *fermions* according to the authors of [11, 15]. The best approximation (red curves) was obtained in [11, 15] (for crystal no. 2) at the Debye coefficient $\beta = 0.026$ mJ mol^{-1} K^{-4} and the Einstein temperatures $\Theta_{E1} = 16$ K and $\Theta_{E2} = 170$ K and (for crystal no. 3) at $\beta = 0.017$ mJ mol^{-1} K^{-4}, $\Theta_{E1} = 24$ K, and $\Theta_{E2} = 160$ K. The solid and dotted green lines represent small Schottky contributions C_{Sch}, different from zero in the range of 1–2 K and obtained for a three-level system with a small splitting $\Delta_1 = 1.4$ K, $\Delta_2 = 6.2$ K and $\Delta_1 = 0.6$ K, $\Delta_2 = 2.2$ K for respective YbB_{12} crystals no. 2 and no. 3 [11, 15]. The values of the coefficient for the linear term in the heat capacity of the narrow-gap semiconductor YbB_{12} found in [11, 15] in the framework of the above procedure are $\gamma \approx 3.8$ mJ mol^{-1} K^{-2}, which corresponds to the 3–4 mJ mol^{-1} K^{-2} found in [25, 26] for an isostructural nonmagnetic reference metal LuB_{12} with a wide (~ 1.6 eV) conduction band [27] and a significant density of electron states $N(E_F)$ [10, 28]. In addition, along with the linear electron component, two Schottky anomalies of a noticeable amplitude in the heat capacity of LuB_{12} were also detected in [26, 29] at low temperatures of 2–40 K, (Fig. 2); as a result, to correctly estimate $N(E_F)$ in this rare earth (RE) dodecaboride with metallic conductivity, the contributions to $C(T)$ have to be separated. We emphasize that, in the heat capacity of all known RE dodecaborides RB_{12} (R–Tb, Dy, Ho, Er, Tm, Lu, and Zr) in the temperature range of 10–80 K, the dominant contribution is from quasilocal vibrations of heavy RE ions with a characteristic Einstein temperature $\Theta_E = 160$–200 K (see, e.g., [10, 25, 26, 29–32]). As a result, to correctly separate the heat capacity components and determine the parameters of the contributions, the $C(T)$ experimental curves for these compounds must be approximated in the wide temperature range of 2–200 K. We also note that the method of inelastic neutron scattering reliably detects a narrow dispersion-free branch in the phonon spectra of RB_{12} at energies of 15–18 meV [33], corresponding to quasilocal vibrations of RE ions in large cavities in the B_{24} cells of a rigid covalent boron framework, while the upper bound of the phonon spectrum significantly exceeds 100 meV ($\Theta_D > 1000$ K) and is

determined by high-frequency vibrations of the boron sublattice.

To verify the results of contribution separation in [11, 15], the authors of [34] carried out precision measurements and analysis of the heat capacity of single-crystal samples of the YbB_{12} semiconductor. It was shown (Fig. 3) that, in the intermediate temperature range of 10–80 K, the heat capacity of YbB_{12} is so high that describing it requires using the sum of the Einstein and Schottky contributions with close energy parameters $\Theta_E \approx \Delta_1 \approx 123$ K; quasilocal vibrations of Yb ions and transitions between levels are both observed in each unit cell of the crystal structure (i.e., the reduced concentrations of Einstein oscillators N_E and Schottky centers N_{Sch1} correspond to the concentration of ytterbium ions $N_E = N_{Sch1} = N_{Yb} = 1$ [34]). We emphasize that, in separating the contributions to the specific heat in [34], the Debye temperature $\Theta_D \approx 1300$ K was used, the value found directly from the data of X-ray diffraction analysis for the root-mean-square atomic displacements of boron atoms in YbB_{12}. According to the approach developed in [26, 29–31], energies $\Delta_1 \approx 123$ K and $\Delta_2 \approx 21$ K are determined by the barrier height in double-well potentials (see the inset to Fig. 3) of two types, caused respectively by charge fluctuations on Yb ions and by boron vacancies. Moreover, in contrast to the total concentration $N_{Sch1} = 1$ recorded for vibrations of Yb ions in a double-well potential in each fcc unit cell of the YbB_{12} crystal structure, the concentration $N_{Sch2} \approx 1.3\%$ corresponds to the fraction of ytterbium ions that are displaced from centrosymmetric positions in the B_{24} cavities due to the presence of vacancies in the boron sublattice in their immediate neighborhood. Because one boron vacancy leads to displacements of the two Yb ions closest to it, taking this component into account in the heat capacity allows estimating the number of boron vacancies as $n_v(B) = N_{Sch2}/2 \approx 0.65\%$, which is in good agreement with their concentration of 1–2% found at low temperatures from measurements of YbB_{12} powders using EXAFS spectroscopy [32].

To compare the absolute value and nature of the variation of the heat capacity of YbB_{12} single crystals investigated in [11, 15] and in our study [34], we carried out detailed measurements of $C(T)$ in the range of 0.4–8 K. Our results, obtained with the same single crystal as in [34], are presented for comparison with the data in [11, 15] (black symbols in Fig. 1). At temperatures of 1–1.5 K, our minimum values of $C/T \approx 3.3$ mJ mol^{-1} K^{-2} are lower than the Sommerfeld coefficient found in [11, 15] by 15% (see Fig. 1), which obviously indicates the predominance of the vacancy low-temperature Schottky contribution to the heat capacity of YbB_{12}. We also note that the Einstein temperature $\Theta_E \approx 123$ K found in [34] from the analysis of heat capacity correlates with both the temperature of spin fluctuations $T_{sf} \approx 11$ meV ≈ 128 K obtained in [35] from an estimate of the peak width in the YbB_{12} quasielastic neutron scattering spectra, and with the value $\Theta_E = 141 \pm 10$ K found in [34] by X-ray diffraction analysis for root-mean-square atomic displacements of ytterbium atoms in this dodecaboride. Thus, the wide-range study of YbB_{12} carried out in [34] in the range of 2–200 K (see Fig. 3) allowed the authors to propose a correct separation of contributions to the heat capacity at intermediate and low temperatures and to conclude that $N(E_F) \sim 0$ at close to zero values of the density of states, which *rules out the possibility of the appearance of gapless uncharged quasiparticles* (*Majorana fermions*) in the dielectric state of this narrow-gap semiconductor with strong electron correlations. We emphasize once again that it was

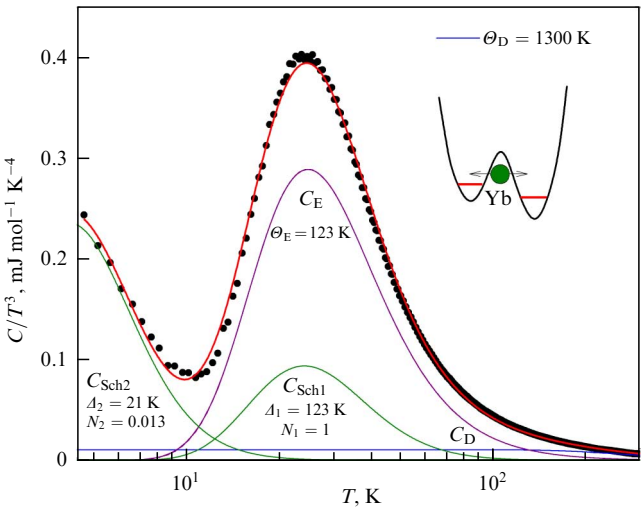

Figure 3. Separation of low-temperature molar heat capacity of YbB_{12} (black dots: experiment, red curve: approximation results) into Debye (C_D), Einstein (C_E), and two Schottky (C_{Sch1} and C_{Sch2}) components. Inset schematically shows quasilocal vibrations of the Yb ion (green ball), accompanied by transitions between energy levels in a double-well potential (constructed in accordance with data in [34]).

precisely the large finite values of the density of quasiparticle states $N(E_F) \neq 0$ obtained in [11, 15] from an incorrectly performed analysis of the heat capacity that led the authors to the conclusion about the existence of *uncharged fermions* in the YbB_{12} gap.

We note that, as shown in previous studies of the magnetic and galvanomagnetic properties of $Tm_{1-x}Yb_xB_{12}$ solid solutions [36, 37] and of EPR in YbB_{12} [38], manybody states in the gap have a filamentary structure and represent conducting channels in the semiconductor matrix. Recent comprehensive studies of high-quality single-domain YbB_{12} crystals performed using precision X-ray diffraction techniques and low-temperature polarization THz-IR spectroscopy, in combination with detailed measurements of magnetoresistance, have allowed establishing the nature of the manybody states in the gap [39]. In particular, it was first shown in [39] that YbB_{12} is actually *a heterogeneous system with electron phase separation on the nanometer scale*, with conducting channels formed in the semiconductor matrix by *dynamical charge stripes*. The authors of [39] emphasize that the detection of dynamical charge stripes in YbB_{12} by several independent experimental methods is of fundamental importance for explaining the nature of the exotic dielectric state in Kondo insulators.

3. Heat capacity of YbB_{12} in a pulsed magnetic field

Among the recent results of heat capacity measurements in YbB_{12}, a unique study performed at low temperatures in pulsed magnetic fields up to 60 T is worth noting [40]. Based on an analysis of experimental data in the extremely narrow temperature range of 1.9–3.3 K in the simplest model and taking only the Debye $C_D = \beta T^3$ and electron γT contributions into account, the authors of [40] concluded that, under an insulator-to-metal transition induced by a magnetic field of about 50 T (Fig. 4a) and accompanied by a sharp increase in magnetization, the Sommerfeld coefficient γ increases by more than an order of magnitude and reaches values

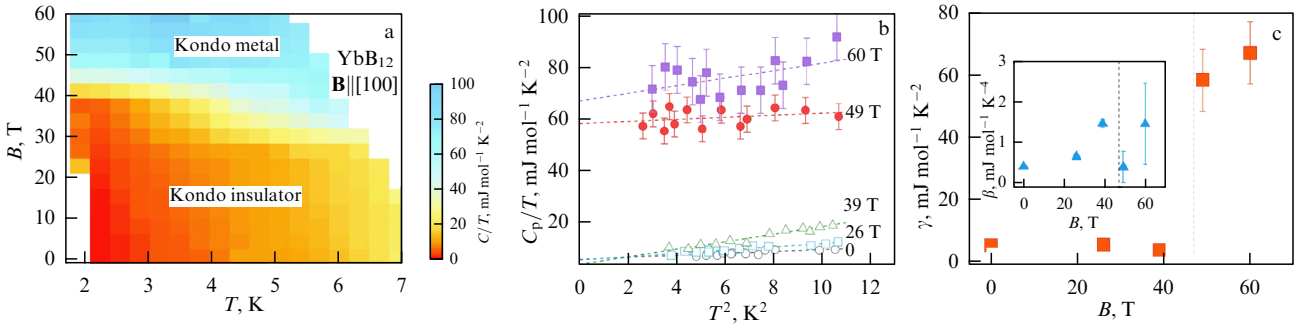

Figure 4. (a) B–T phase diagram of YbB_{12}. Color coding shows heat capacity C/T for $\mathbf{B}||[100]$. (b) Temperature dependence $C/T = f(T^2)$ in magnetic fields up to 60 T. Dotted lines show the linear least-square fit to experimental data. (c) Dependence of linear coefficient γ on the magnetic field. Inset shows dependence of coefficient β of Debye heat capacity $C_D = \beta T^3$ on the magnetic field (from [40]).

$\gamma \approx 67$ mJ mol^{-1} K^{-2} at 60 T (Fig. 4b, c). We note that, in a zero magnetic field, the value of the Debye coefficient $\beta = 0.4$ mJ mol^{-1} K^{-4} obtained from such an analysis (see the inset to Fig. 4c) is approximately 20 times (!) higher than that found in [11, 15]. The value of β corresponds to the Debye temperature $\Theta_D \approx 388$ K, which is approximately one third the values typical of RB_{12}, $\Theta_D \sim 1100$–1300 K, caused by thermal vibrations of the light boron framework. In addition, the large values of the linear heat capacity coefficient found in the framework of the procedure proposed in [40] (Fig. 4c), according to the authors, indicate a transition in a strong magnetic field to the Kondo-metal phase with heavy fermions (Fig. 4a). According to [40], under the transition to the metallic state, a significant increase in magnetization induced by the external magnetic field should also indicate a sharp increase in the density of states $N(E_F)$ associated with the formation of a manybody Kondo resonance at E_F and hence with the appearance of heavy fermions in the metal phase of YbB_{12}.

Unfortunately, in contrast to the measurements in [40], which are unique in their complexity and apparently provide reliable experimental data, the analysis of the results proposed in the same study does not stand up to criticism. Indeed, as was shown above, the simplest model chosen for the analysis in [40] does not correspond to the physical processes in YbB_{12}, because, in the range of 1.9–3.3 K used by the authors, the Schottky contribution C_{Sch1} is actually dominant in the heat capacity (see Fig. 3), while the Sommerfeld term is close to zero in this narrow-gap semiconductor. Thus, the value $\gamma \approx 5$ mJ mol^{-1} K^{-2} obtained in [40] in the zero field, which is huge for a semiconductor, as in the case of the analysis proposed in [11, 15] (see Fig. 1), is erroneous. In addition, a more than 10-fold increase in the coefficient γ discovered in [40] for the insulator-to-metal transition near 50 T (Fig. 4c) is also a consequence of incorrect modeling of the heat capacity curves. We note that the problem of the emergence of 'false' heavy fermions under the transition to a state with magnetic moments and magnetic clusters, including the spin glass phase, was studied in detail more than 25 years ago by Schneidner et al. [41] and Coles [42]. In particular, it was shown in [41, 42] that the cause of a sharp increase in the low-temperature heat capacity, which is often incorrectly interpreted in terms of an increase in the effective mass of conduction electrons, is the appearance of an additional Schottky contribution. Such a magnetic Schottky anomaly in the heat capacity intensifies as the external magnetic field increases and moves upward along the temperature scale [41, 42], as has been reliably detected for YbB_{12} by the authors of [11, 15].

4. Hall effect in YbB_{12}

Recently, in [43], the Hall effect was studied in detail on single-crystal YbB_{12} samples in the wide temperature range of 0.35–50 K in steady (up to 18 T) and pulsed (up to 60 T) magnetic fields. The measurements in [43] followed a scheme traditional for a Hall experiment, with two directions of the field $(-H, +H)$ oriented along the normal $\mathbf{H}||\mathbf{n}||[100]$ to the lateral surface of the crystal (Fig. 5a). An analysis of the measurement results (see, e.g., Fig. 5c), according to the authors of [43], definitely confirms the two-fluid scenario of charge transport in YbB_{12}, with two types of fermions involved: a *charge-neutral Fermi liquid* (*Majorana fermions*) and ordinary incoherent charge carriers; these two components actively interact with each other. Because the conclusion made by the authors of [43] about the transport of uncharged fermions is based on, among other arguments, the above-discussed methodologically erroneous estimates of the quasiparticle contribution to the YbB_{12} heat capacity (see Fig. 1–4), it is of more interest here to dive deeper into an analysis of the contributions to the signal measured from Hall contacts in RE dodecaborides, including the nonmagnetic reference compound LuB_{12} [44], substitutional solid solutions $Ho_xLu_{1-x}B_{12}$ [45] and $Tm_{1-x}Yb_xB_{12}$ [36, 46], and YbB_{12} itself.

We first note that, in all RE dodecaborides, the cooperative Jahn–Teller structural instability of the boron framework leads to electron phase separation caused by the formation of dynamical charge stripes along the ⟨110⟩ directions in the fcc lattice (Fig. 6a and [47, 10]). The authors of [44, 45] showed that, for both LuB_{12} and $Ho_xLu_{1-x}B_{12}$, the interaction of quantum electron density fluctuations (stripes) with a perpendicular external magnetic field $\mathbf{H}||[100]$ at intermediate and low temperatures sharply renormalizes the Hall resistance. This interaction gives rise to an anomalous topological contribution $\rho_H^{an}(\varphi)$ with a positive sign, which is reliably detected when measuring the angular dependences of the Hall resistance (see the diagram in Fig. 5b and experimental data in Fig. 6b, c [44] and Fig. 7b [45]). We note that, for an isotropic conductor, a change in the direction of the external magnetic field relative to the normal to the lateral surface of the sample (Fig. 5b) causes the behavior of the Hall resistance of the form $\rho_H = \rho_{H0}\cos\varphi$, associated with a corresponding change in the projection of $\mathbf{H}$ onto the direction of the normal to the crystal. Dependences of this type are reliably detected both in LuB_{12} in low fields and at high temperatures (Fig. 6b, c), and in $Ho_{0.8}Lu_{0.2}B_{12}$ at $T > 60$ K (Fig. 7a). As can be seen

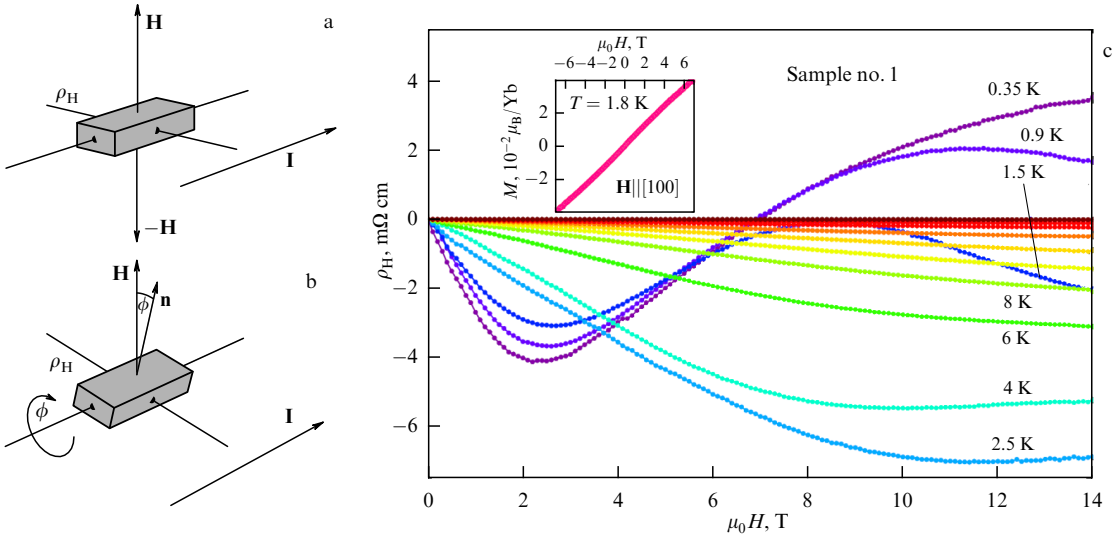

Fig. 5. Schematic views for measuring Hall resistance ρ_H: (a) in the traditional method for two opposite directions of the external magnetic field along the normal to the lateral surface of the crystal and (b) when recording angular dependence $\rho_H(\varphi)$ for a sample rotating in a steady field. (c) Field dependence of Hall resistance $\rho_H(H, T_0) = (\rho_{xy}(+H) - \rho_{xy}(-H))/2$ measured in magnetic field **B**||[100] up to 14 T in the temperature range of 0.35–50 K for a single-crystal YbB_{12} sample. Inset shows magnetization M of the sample depending on the magnetic field in the range from −7 to +7 T at 1.8 K (from [43]).

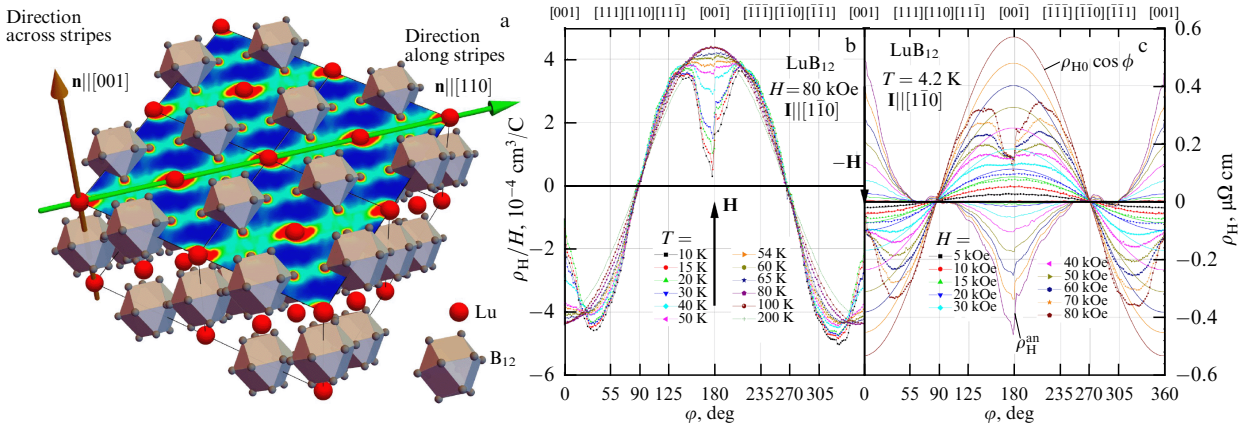

Figure 6. (a) Crystal structure of RB_{12}. Colored plane shows a map of total electron density on the (001) face obtained by the maximum entropy method when analyzing results of X-ray diffraction measurements (see [47]). Green bars correspond to dynamical charge stripes. Green and brown arrows, respectively, show the directions along (**n**||[110]) and across (**n**||[001]) stripes. Angular dependences of Hall resistance $\rho_H(\varphi)$ (symbols) measured when the sample is rotated such that the magnetic field direction varies in the **H**||(1 − 10) plane and the corresponding model curves $\rho_{H0}\cos\varphi$ (thin lines) for a single-crystal LuB_{12} sample with a normal to the lateral surface **n**||[001] (b) in the temperature range of 10–200 K in a magnetic field $\mu_0 H = 8$ T and (c) at $T = 4.2$ K in a magnetic field up to 8 T (in accordance with the results in [44]). Thick lines show anomalous anharmonic contribution $\rho_H^{an}(\varphi)$. Vertical arrows show directions (−**H**, +**H**) corresponding to measurements of the Hall effect in the traditional setup with two opposite orientations of the magnetic field (Fig. 5a); top axis shows crystallographic directions.

from Fig. 6b, c and Fig. 7b, in strong fields at low temperatures, a positive-sign anomalous contribution $\rho_H^{an}(\varphi)$ appears on the angular curves in a wide range of angles in the vicinity of **H**||[001], sharply reducing the amplitude of the signal measured from the Hall contacts. In such a situation, measurements in the traditional setup with two opposite orientations of the magnetic field (−**H**, +**H**) do not allow separating the normal and anomalous contributions, which leads to incorrect estimates of the Hall concentration and an incorrect analysis of the temperature and field curves of the Hall resistance.

Apparently, much more difficult is the task of separating the contributions to electron transport in RE dodecaborides containing ytterbium ions. In this case, along with the electron phase separation (stripes along ⟨110⟩) caused by the Jahn–Teller structural instability of the boron framework [10, 47], charge and spin fluctuations due to the dynamical mixed valence of Yb are effective on the ytterbium ions in RB_{12} (see, e.g., [10, 46]). Studies [36, 46] of the Hall effect in substitutional $Tm_{1-x}Yb_xB_{12}$ solid solutions showed that, in the temperature range $T < \Theta_E \sim 150$ K in strong magnetic fields, along with the usual isotropic harmonic Hall component $\rho_{xy} = \rho_{H0}\cos\varphi$, a transverse even resistive component ρ_{TE} also appears on angular curves $\rho_H(\varphi)$ and sharply increases as the temperature decreases (transverse even effect; see, e.g., [48]). As an example, in Figs 8a, b, we show typical angular dependences obtained in measuring the resistance from Hall contacts in $Tm_{1-x}Yb_xB_{12}$ solid solutions with $x = 0.54$ and $x = 0.72$ and also present the results of the separation of contributions (see [36] for more details). We emphasize that the even component of the $\rho_{TE}\cos(2\varphi)$ signal in $Tm_{1-x}Yb_xB_{12}$ Hall measurements was shown in [36]

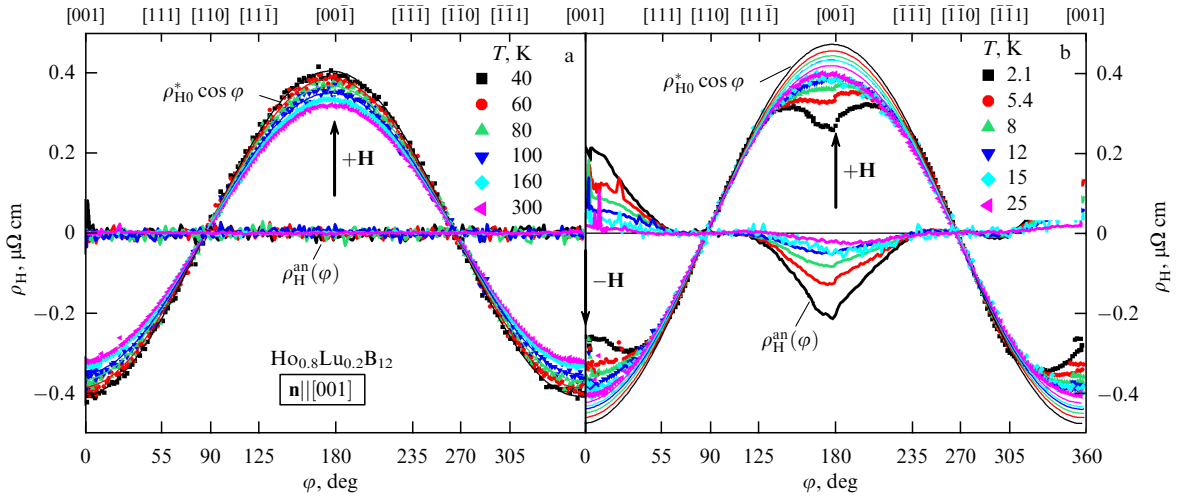

Figure 7. Angular dependences of Hall resistance $\rho_H(\varphi)$ (symbols) measured when a sample is rotated such that the magnetic field direction varies in the **H**||(110) plane and related model curves $\rho_{H0}\cos(\varphi)$ (thin lines) for a single-crystal $Ho_{0.8}Lu_{0.2}B_{12}$ sample with a normal to the lateral surface **n**||[001] in the temperature range of 2.1–300 K in the magnetic field $\mu_0 H = 8$ T corresponding to the paramagnetic state (in accordance with results in [45]). Thick lines show anomalous anharmonic contribution $\rho_H^{an}(\varphi)$. Vertical arrows show directions $(-\mathbf{H}, +\mathbf{H})$ corresponding to Hall effect measurements in the traditional setup with two opposite magnetic field orientations; top axis shows crystallographic directions.

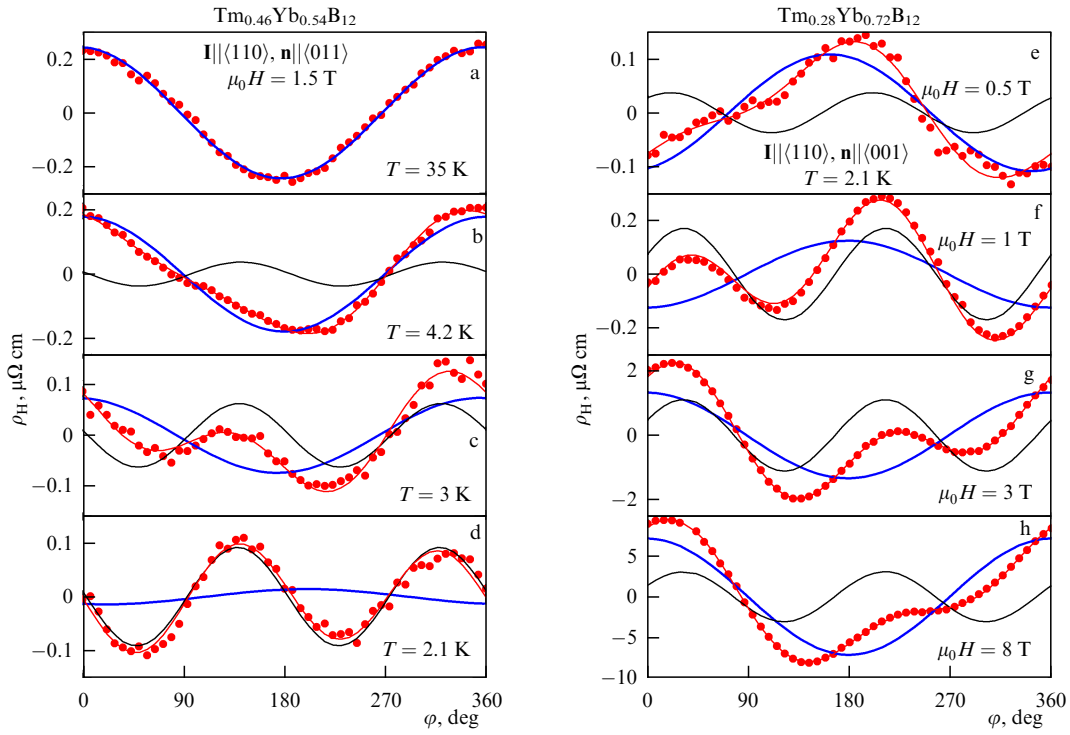

Figure 8. (a) Angular dependences of Hall resistance $\rho_H(\varphi)$ (red dots) for single-crystal samples of (a–d) $Tm_{0.46}Yb_{0.54}B_{12}$ in magnetic field $\mu_0 H = 1.5$ T at various temperatures in the range of 2–35 K and (e–h) $Tm_{0.28}Yb_{0.72}B_{12}$ at $T = 2.1$ K in magnetic fields up to 8 T (in accordance with results in [36]). For all experimental $\rho_H(\varphi)$ curves, Figs a–h show decomposition into odd Hall contribution $\rho_{xy}(\varphi) \sim \cos(\varphi)$ (blue curve) and transverse even resistive effect $\rho_{TE} \sim \cos(2\varphi)$ (black curve) along with the common envelope (red curve).

to be unrelated to the parasitic component from the magnetoresistance, which arises in the case of an asymmetric arrangement of Hall contacts on the sample. We also note that the transverse even effect ρ_{TE} was observed previously in the normal state of high-temperature superconductors (HTSCs) and was related to the appearance of stripes on the surface and in the layers of HTSC crystals [49, 50].

Thus, for YbB_{12} in strong magnetic fields at low temperatures, we should expect the signal from Hall contacts to the single-crystal sample to contain not only the usual harmonic component ρ_{xy} but also the transverse even resistive effect ρ_{TE} (second harmonic signal) and the anomalous topological positive-polarity contribution ρ_H^{an} (see Figs 6–8), both induced by stripes. It is obvious that the correct separation of contributions is possible only by analyzing the angular curves of the Hall signal (see the experimental diagram in Fig. 5b). To check the presence of several contributions to the $\rho_H(\varphi)$ signal measured from Hall contacts, we should consider angular measurements of the Hall resistance in the field $\mu_0 H = 8$ T (Fig. 9a), as well as the

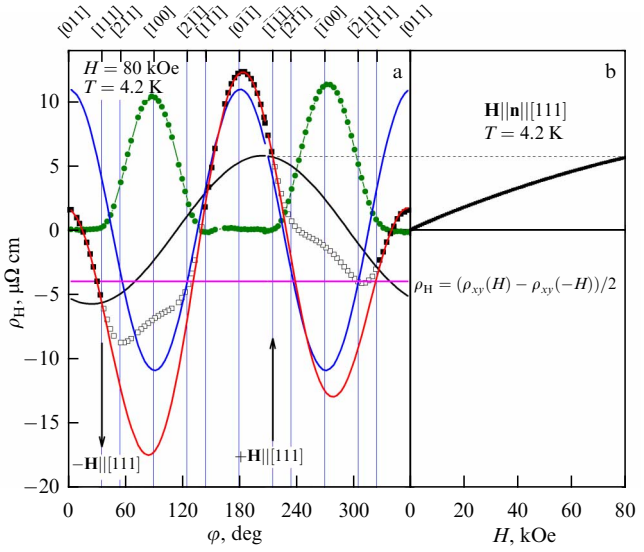

Figure 9. (a) Angular dependence of Hall resistance $\rho_H(\varphi)$ at $T = 4.2$ K in magnetic field $H = 80$ kOe (black squares) measured when the sample rotates such that the magnetic field direction varies in the **H**||(110) plane for a YbB_{12} single crystal with a normal to the lateral surface **n**||[111] (see the experimental diagram in Fig. 5b). Black, blue, and green solid lines, respectively, show odd Hall contribution ρ_H, transverse even effect ρ_{TE}, and anomalous Hall effect ρ_H^{an} due to stripes; red line in the range of approximation angles (solid black squares) shows the common envelope of these contributions. Vertical arrows mark directions $(-\mathbf{H}, +\mathbf{H})$ along the normal **H**||**n**||[111]; top axis shows crystallographic directions. (b) Field dependence of Hall resistance measured at $T = 4.2$ K for two field directions $(-\mathbf{H}, +\mathbf{H})$ along the normal **H**||**n**||[111]. Horizontal dotted line shows the correspondence between amplitude of the Hall contribution ρ_H found in measuring (a) the angular dependence and (b) field curves $\rho_H = (\rho_{xy}(+H) - \rho_{xy}(-H))/2$.

field dependence data $\rho_H(H)$ (Fig. 9b) for a single-crystal YbB_{12} sample in the **H**||**n**||[111] orientation at $T = 4.2$ K. We chose just that orientation, because the anomalous topological contribution ρ_H^{an} to the Hall signal was shown in [44, 45] to vanish for RE dodecaborides for the **H**||[111] direction. As can be seen from Fig. 9a, the obtained result of angular measurements confirms the presence of three angle-dependent components $\rho_H(\varphi) = \rho_{xy}(\varphi) + \rho_{TE}(\varphi) + \rho_H^{an}(\varphi)$ in the YbB_{12} Hall signal. We emphasize that the contributions of the second harmonic $\rho_{TE} \sim \cos(2\varphi)$ and the anomalous component ρ_H^{an} to the Hall resistance are comparable in amplitude with the standard Hall component ρ_{xy} (Fig. 9a). Hence, we can conclude that all three contributions must be properly separated and subsequently analyzed separately. We also note that the ρ_H^{an} contribution associated with stripes is observed in a wide neighborhood of **H**||⟨100⟩, as for other RB_{12} (see Figs 6, 7), while ρ_H measured in the scheme with sample rotation in a magnetic field in the **H**||[111] orientation (Fig. 9a) coincides, with good accuracy, with the result of traditional field measurements (Fig. 9b). Thus, the analysis of the results of Hall effect measurements in YbB_{12} proposed in [43] should be pronounced incorrect, because the presence in the Hall signal of three different components dependent on the field direction was not taken into account in that analysis. The conclusion of the authors of [43] regarding the presence of a *charge-neutral Fermi liquid* (*Majorana fermions*) in this narrow-gap semiconductor with strong electron correlations is therefore also unfounded.

5. Conclusions

We analyzed the results of heat capacity measurements [11, 15, 40] and Hall effect measurements [43] in the Kondo insulator YbB_{12}. We have shown that the approaches to separating the contributions to thermal and transport characteristics proposed by the authors of these studies are incorrect and lead to unfounded conclusions about the presence of a *charge-neutral Fermi liquid* (*Majorana fermions*) in this model narrow-gap semiconductor with strong electron correlations and electron phase separation. A consistent explanation of the experimental data is possible in the framework of the concept of the filamentary structure of conducting channels in the semiconductor matrix of ytterbium-based dodecaborides [36, 39]. Such channels represent electron density inhomogeneities on the nanometer scale, resulting from the formation of dynamical charge stripes that form manybody states near the Fermi level.

The study was carried out with financial support from the Russian Science Foundation, project no. 22-22-00243. The authors are grateful to N B Bolotina, N Yu Shitsevalova, V B Filipov, V V Glushkov, and B P Gorshunov for the useful discussions.

References

1. Lu F et al. *Phys. Rev. Lett.* **110** 096401 (2013)
2. Weng H M et al. *Phys. Rev. Lett.* **112** 016403 (2014)
3. Hagiwara K et al. *Nat. Commun.* **7** 12690 (2016)
4. Iga F et al. *Solid State Commun.* **50** 903 (1984)
5. Kasuya T et al. *J. Magn. Magn. Mater.* **31–34** 447 (1983)
6. Yamaguchi J et al. *Phys. Rev. B* **79** 125121 (2009)
7. Hagiwara K et al. *J. Phys. Conf. Ser.* **807** 012003 (2017)
8. Rousuli A et al. *J. Phys. Condens. Matter* **29** 265601 (2017)
9. Iga F, Shimizu N, Takabatake T *J. Magn. Magn. Mater.* **177–181** 337 (1998)
10. Sluchanko N E, in *Rare-Earth Borides* (Ed. D S Inosov) (Singapore: Jenny Stanford Publ., 2021) p. 331; arXiv:2004.06371
11. Sato Y *Quantum Oscillations and Charge-Neutral Fermions in Topological Kondo Insulator* YbB_{12} (Springer Theses) (Singapore: Springer, 2021) https://doi.org/10.1007/978-981-16-5677-4
12. Xiang Z et al. *Nat. Phys.* **17** 788 (2021)
13. Xiang Z et al. *Science* **362** 65 (2018)
14. Sato Y et al. *J. Phys. D* **54** 404002 (2021)
15. Sato Y et al. *Nat. Phys.* **15** 954 (2019)
16. Coleman P, Miranda E, Tsvelik A *Physica B* **186–188** 362 (1993)
17. Coleman P, Miranda E, Tsvelik A *Phys. Rev. B* **49** 8955 (1994)
18. Coleman P, Ioffe L B, Tsvelik A M *Phys. Rev. B* **52** 6611 (1995)
19. Erten O et al. *Phys. Rev. Lett.* **119** 057603 (2017)
20. Varma C M *Phys. Rev. B* **102** 155145 (2020)
21. Heath J T, Bedell K S *J. Phys. Condens. Matter* **32** 485602 (2020)
22. Sodemann I, Chowdhury D, Senthil T *Phys. Rev. B* **97** 045152 (2018)
23. Chowdhury D, Sodemann I, Senthil T *Nat. Commun.* **9** 1766 (2018)
24. Rao P, Sodemann I *Phys. Rev. B* **100** 155150 (2019)
25. Czopnik A et al. *J. Phys. Condens. Matter* **17** 5971 (2005)
26. Bolotina N B et al. *J. Phys. Chem. Solids* **129** 434 (2019)
27. Okamura H et al. *Phys. Rev. B* **62** R13265 (2000)
28. Jäger B et al. *J. Phys. Condens. Matter* **18** 2525 (2006)
29. Sluchanko N et al. *J. Supercond. Nov. Magn.* **26** 1663 (2013)
30. Czopnik A et al. *J. Solid State Chem.* **177** 507 (2004)
31. Azarevich A et al. *Phys. Rev. B* **103** 104515 (2021)
32. Menushenkov A P et al. *JETP Lett.* **98** 165 (2013); *Pis'ma Zh. Eksp. Teor. Fiz* **98** 187 (2013)
33. Rybina A V et al. *Phys. Rev. B* **82** 024302 (2010)
34. Bolotina N et al. *Acta Cryst. B* **76** 1117 (2020)
35. Alekseev P A et al. *Phys. Rev. B* **89** 115121 (2014)
36. Sluchanko N E et al. *J. Exp. Theor. Phys.* **115** 509 (2012); *Zh. Eksp. Teor. Fiz.* **142** 574 (2012)

37. Bogach A V et al. *J. Exp. Theor. Phys.* **116** 838 (2013); *Zh. Eksp. Teor. Fiz.* **143** 965 (2013)
38. Altshuler T S et al. *Phys. Rev. B* **68** 014425 (2003)
39. Azarevich A et al. *Chinese Phys. Lett.* **39** 127302 (2022)
40. Terashima T T et al. *Phys. Rev. Lett.* **120** 257206 (2018)
41. Gschneidner K A (Jr.) et al. *Physica B* **163** 507 (1990)
42. Coles B R *Physica B* **223–224** 260 (1996)
43. Xiang Z et al. *Phys. Rev. X* **12** 021050 (2022)
44. Sluchanko N et al. *Phys. Rev. B* **103** 035117 (2021)
45. Khoroshilov A L et al. *Molecules* **28** 676 (2023)
46. Sluchanko N E et al. *J. Phys. Condens. Matter* **31** 065604 (2019)
47. Bolotina N B et al., in *Rare-Earth Borides* (Ed. D S Inosov) (Singapore: Jenny Stanford Publ., 2021) p. 293; arXiv:2010.16239
48. Hurd C M *Adv. Phys.* **23** 315 (1974)
49. Koblischka M R, Winter M, Hartmann U *Supercond. Sci. Technol.* **20** 681 (2007)
50. Janeček I, Vašek P, cond-mat/0306560